Qualifying Examination Part II

Title:

"Accurate residual stress measurement as a function of depth in environmental barrier coatings via a combination of X-ray diffraction and Raman spectroscopy"

Authors: Cheng Ye & Peng Jiang
Journal: Ceramics International
Publication Date: February 04, 2020

Bryant Kanies
09/10/2020

Outline

- Introduction
- Background & Underlying Mechanisms
  - Ceramic Matrix Composites
  - Protective Coatings
  - Residual Stress in Coatings
  - X-Ray Diffraction – The $Sin^2\Psi$ Method
  - Raman Piezospectroscopy
- Summary of Work
- Critical Review
  - Insufficient Background
  - Reproducibility
  - Accuracy
  - Novelty & Impact
  - Suggested Improvements
- Conclusions

Introduction

- Several industries require critical components to function correctly in harsh environments for thousands of hours
- Operation at high temperatures improves process efficiencies
  - Fusion reactors >1000 °C
  - Very High Temperature Reactors ~1500 °C
  - Aerospace applications ~2000 °C
- Ni-based superalloys are traditional solution
  - Limited to 900 – 1100 °C
- High temperature ≥1200 °C

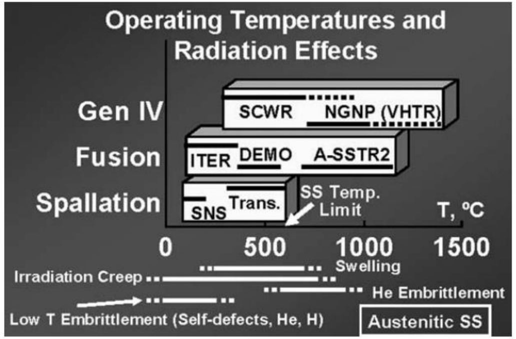

From: [2]

Introduction

- Ceramics maintain satisfactory mechanical, tribological, chemical, and physical properties at elevated temperatures
- Typically brittle, flaw-sensitive, and lack toughness
  - Catastrophic failure modes & damage during fabrication and service
- Two solutions for high temperatures:
  - Thermal Barrier Coatings (TBCs)
    - Thermal insulation for substrates
  - Ceramic Matrix Composites (CMCs)
    - Maintain ideal ceramic properties
    - Offer higher toughness than monolithic ceramics

Reference(s): 8, 14-21

Introduction

- Problem: CMCs & TBCs face corrosion & phase instability
  - Water vapor & calcium-magnesium-alumino silicates (CMAS)
  - $\geq$ 1100-1200 °C
- Proposed Solution: <u>Environmental Barrier Coatings (EBCs)</u>
- EBCs must maintain integrity through operating conditions
- Residual stresses in EBCs lead to failure
- Characterization of residual stresses is crucial

Reference(s): 8, 14-21

Outline

- Introduction
- Background & Underlying Mechanisms
  - Ceramic Matrix Composites
  - Protective Coatings
  - Residual Stress in Coatings
  - X-Ray Diffraction – The $Sin^2\Psi$ Method
  - Raman Piezospectroscopy
- Summary of Work
- Critical Review
  - Insufficient Background
  - Reproducibility
  - Accuracy
  - Novelty & Impact
  - Suggested Improvements
- Conclusions

Ceramic Matrix Composites

- Ceramic matrix reinforced through incorporation of fibers
- Fiber preform filled with matrix material

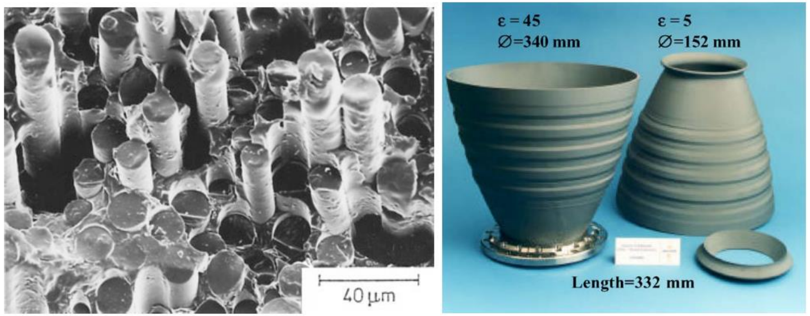

Figure from [15] & [27]

- Common types:
  - SiC/SiC & C/SiC
  - Nicalon/Nicalon glass
  - Al_2O_3/Al_2O_3
- Usage:
  - Exhaust cones
  - Nose cap of X-38 return vehicle
  - Shrouds & airfoils
  - Brake pads
  - First wall blanket in fusion reactors
  - Cutting tool inserts
  - Ceramic composite filters

Reference(s): 8, 9, 15, 22-27

Ceramic Matrix Composites

- Ceramics' brittle nature and porosity lead to catastrophic failure
- Strengthening Mechanisms:
  - Compressive prestressing
  - Impeding crack propagation
  - Fiber pullout
  - Crack deflection
  - Phase transformation toughening
- Al_2O_3 CMC vs. Monolithic
  - 8-8.5 MPa $m^{1/2}$ vs. 4-5 MPa $m^{1/2}$
  - 20 volume-% SiC whiskers

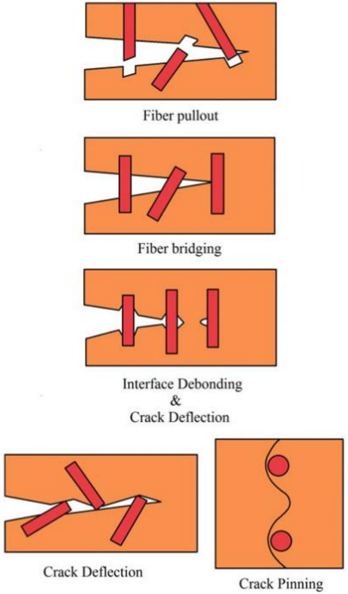

Figure from [15]

Reference(s): 8, 9, 15, 22-27

Protective Coatings

- EBCs & TBCs are very similar
  - TBCs extend component lifetime through thermal insulation
  - EBCs enhance corrosion resistance
  - Structure: Topcoat, intermediate layers / bond coat, thermally grown oxide (TGO), substrate
    - MCrAlY alloy, Si, mullite, or SiC as bond coat
- Deposition:
  - Chemical vapor deposition (CVD)
  - Slurry dip/spin
  - Electron beam-Physical Vapor Deposition (EB-PVD)
  - Atmospheric Plasma Spraying (APS)

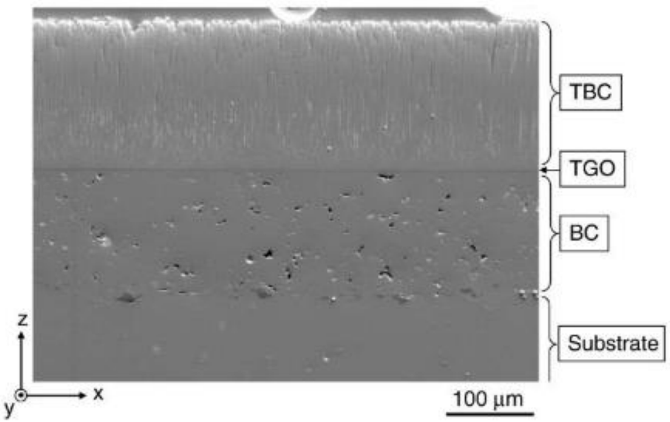

A 4 mole-% YSZ TBC demonstrating a typical structure from [32]

Reference(s): 8,16,17,21,28-39

Protective Coatings

Property	Purpose
High melting point	Operation in high temperature environment
Low thermal conductivity	Thermal insulation of substrate [a]
CTE match with substrate	Dissimilar expansion causes residual stress
Phase stability over operating range	Phase changes may contribute to residual stresses
Chemically inert	Oxidation and corrosion resistance [b]
Chemical compatibility with substrate	Reaction with substrate may lead to precipitates or phases with undesired properties
Low sintering rate	Densification of porous ceramic may change coating properties
Low density	Low weight is often desired in high temperature applications

a – EBCs may not be required to serve as thermal insulators if the substrate can withstand operation temperature

b – TBCs may not be exposed to reactive chemicals depending on the application

Reference(s): 8, 16-19

Residual Stresses

- Influence corrosion resistance, adhesion, & tribological properties
- Cracking & buckling
  - Delamination & Spallation
- Failure exposes substrate to environment
  - Water vapor, high temperatures, CMAS attack
- Measurement:
  - Nanoindentation
  - Curvature measurement
  - X-ray diffraction
  - Raman & photo-stimulated luminescence piezospectroscopy

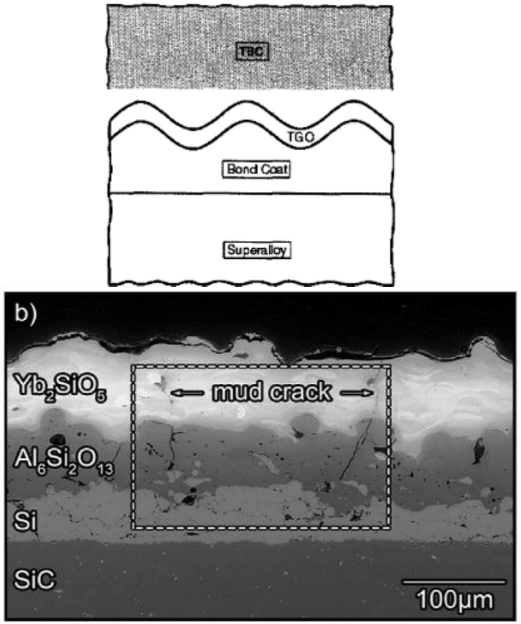

Figures from [17], [18]

Reference(s):17,18,20,31,32,41-47

X-Ray Diffraction: The Sin² Ψ Technique

- Lattice plane used as in-situ strain gauge
  - Plane (hkl)
  - Spacing $d_{hkl} \approx d_{\Phi\Psi}$
  - $2\theta \geq 125°$
- Acquire diffraction peaks by varying source angle Ω
  - $\Psi = \theta - \Omega$
- Stress is slope of ε vs. $Sin^2\Psi$
  - ν = Poisson's ratio, E = Young's Modulus, σ = stress

$$\varepsilon = \frac{d_{\phi\Psi} - d_0}{d_0} = \frac{1+\nu}{E}\sigma_\phi \sin^2\Psi - \frac{\nu}{E}(\sigma_{11} + \sigma_{22})$$

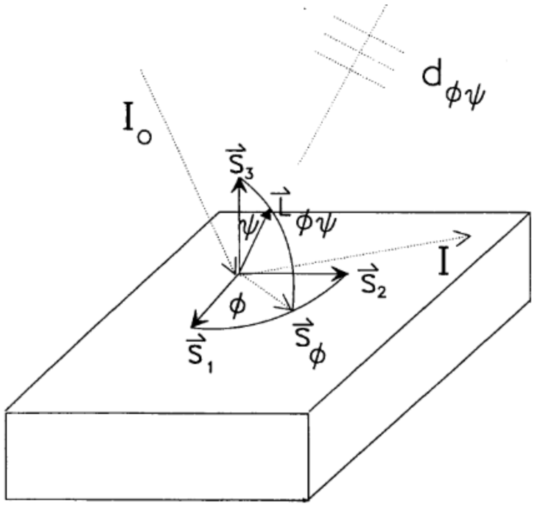

Figure from [48]

Reference(s):20,40,48,49

X-Ray Diffraction: The Sin² Ψ Technique

- Lattice plane used as in-situ strain gauge
  - Plane (hkl)
  - Spacing $d_{hkl} \approx d_{\Phi\Psi}$
  - $2\theta \geq 125°$
- Acquire diffraction peaks by varying source angle Ω
  - $\Psi = \theta - \Omega$
- Stress is slope of ε vs. $Sin^2\Psi$
  - ν = Poisson's ratio, E = Young's Modulus, σ = stress

$$\varepsilon = \frac{d_{\phi\Psi} - d_0}{d_0} = \frac{1+\nu}{E}\sigma_\phi \sin^2\Psi - \frac{\nu}{E}(\sigma_{11} + \sigma_{22})$$

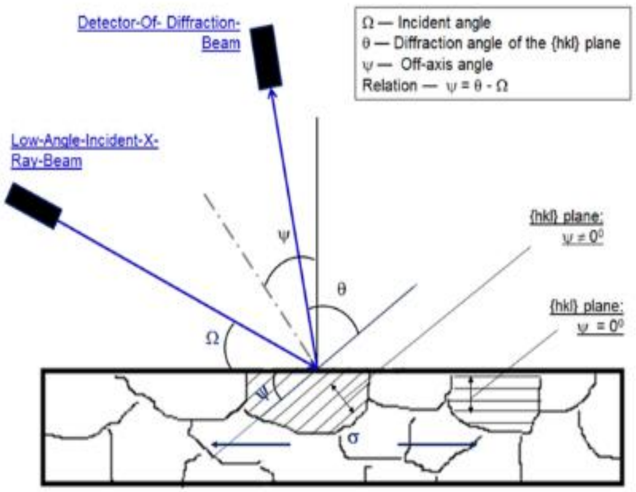

Figure from [40]

Reference(s):20,40,48,49

Raman Piezospectroscopy

$$\Delta\nu = \mathbf{\Pi}_{ij}\boldsymbol{\sigma}_{\mathbf{ij}}$$
$$\Rightarrow \Delta\nu = \Pi\langle\sigma\rangle$$

- Raman spectra:
  - Laser is Raman (inelastically) scattered off a sample
  - Intensity of reflected light vs. Raman shift
- Piezo-spectroscopic effect: stress-induced shift of peak frequency ($\Delta\nu$)
  - Properly: $\mathbf{\Pi}_{\mathbf{ij}}$ - Piezo-spectroscopic (PS) tensor, $\boldsymbol{\sigma}_{ij}$ - stress tensor
  - Randomly oriented grains: Π (PS coefficient) & σ are averages
- Usually requires calibration sample

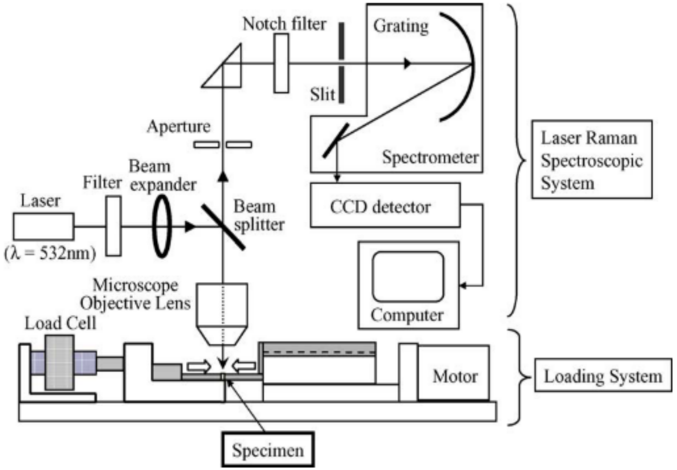

Figure from [55]

Raman Piezospectroscopy

- Raman spectra:
  - Laser is Raman (inelastically) scattered off a sample
  - Intensity of reflected light vs. Raman shift
- Piezo-spectroscopic effect: stress-induced shift of peak frequency ($\Delta\nu$)
  - Properly: $\mathbf{\Pi_{ij}}$ - Piezo-spectroscopic (PS) tensor, $\boldsymbol{\sigma_{ij}}$ - stress tensor
  - Randomly oriented grains: Π (PS coefficient) & σ are averages
- Usually requires calibration sample

$$\Delta\nu = \boldsymbol{\Pi_{ij}}\boldsymbol{\sigma}_{\mathbf{ij}}$$
$$\Rightarrow \Delta\nu = \Pi\langle\sigma\rangle$$

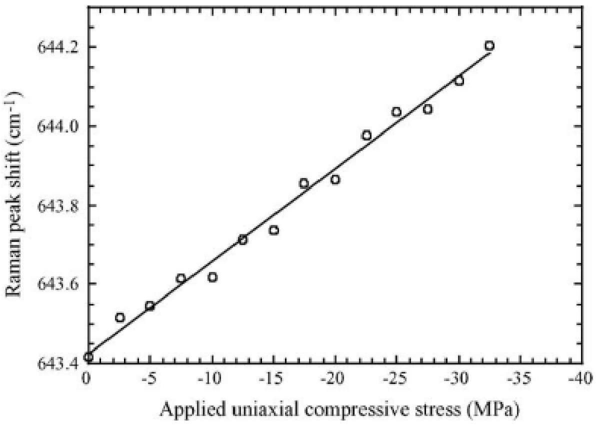

Figure from [55]

Outline

- Introduction
- Background & Underlying Mechanisms
  - Ceramic Matrix Composites
  - Protective Coatings
  - Residual Stress in Coatings
  - X-Ray Diffraction – The $Sin^2\Psi$ Method
  - Raman Piezospectroscopy
- Summary of Work
- Critical Review
  - Insufficient Background
  - Reproducibility
  - Accuracy
  - Novelty & Impact
  - Suggested Improvements
- Conclusions

Deposition of EBCs on CMCs

- EBC:
  - Slurry coating, 80 µm thick
  - 90 mass-% Ytterbium disilicate (YbDS, $Yb_2Si_2O_7$)
  - 10 mass-% Barium strontium aluminosilicate
    - BSAS or $Ba_{0.5}Sr_{0.5}Al_2Si_2O_8$
    - Lower sintering temperature
  - SiC bond coat (40 µm)
- CMC:
  - Chemical vapor infiltration (CVI) = CVD
  - 40 x 5 x 3.5 mm
  - C/SiC

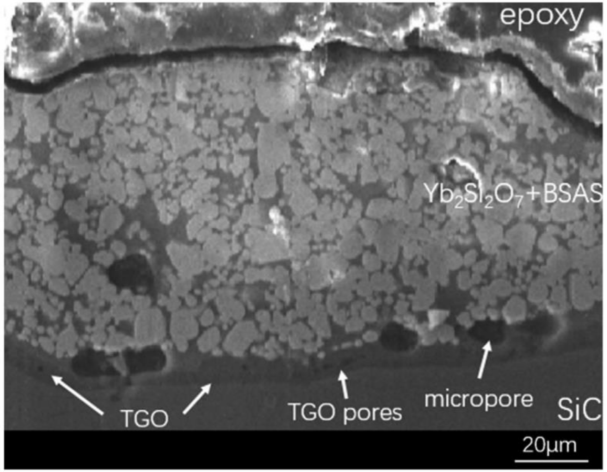

Testing & Sectioning

- High temperature corrosion test:
  - Aluminum oxide (Al_2O_3) tube furnace
  - 50% water vapor and 50% oxygen
  - 1250 °C for 50-hours
- Sectioning:
  - Wrapped in resin, cut with a diamond wire saw, & polished
  - Downward cutting speed of 3 mm/h
  - 10 x 5 x 3.5 mm cross-section pieces
  - SEM image of the cross section

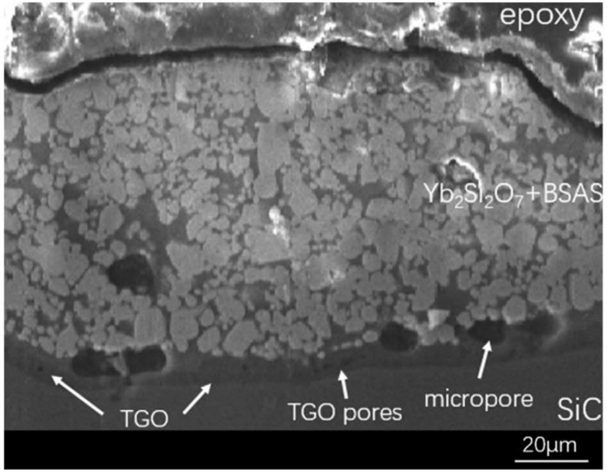

Reference(s): 22

Raman Spectroscopy

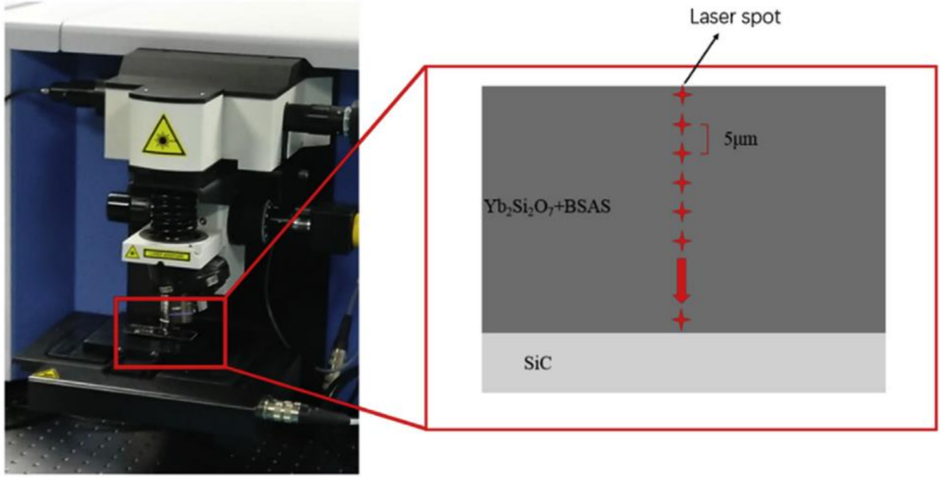

- LaRAM HR Evolution HORIBA
- 633 nm He/Ne laser set to 25% power
    - Reduce error from temperature rise and good signal-to-noise ratio
    - Constant temperature 298 K ± 1 K
- 5 s/scan
- Standard deviation from three different positions at each depth
- Measurements exclusively in the YbDS

Reference(s): 22

Raman Spectroscopy

- 921 cm^{-1} peak
- Lorentzian fit with Labspec5
- Stress-free peak position from YbDS powder used for the coating

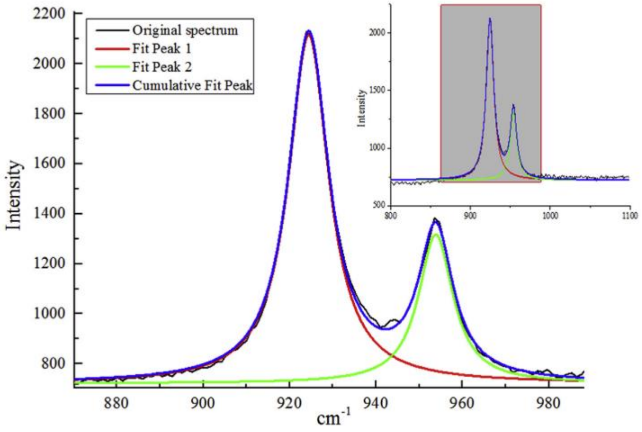

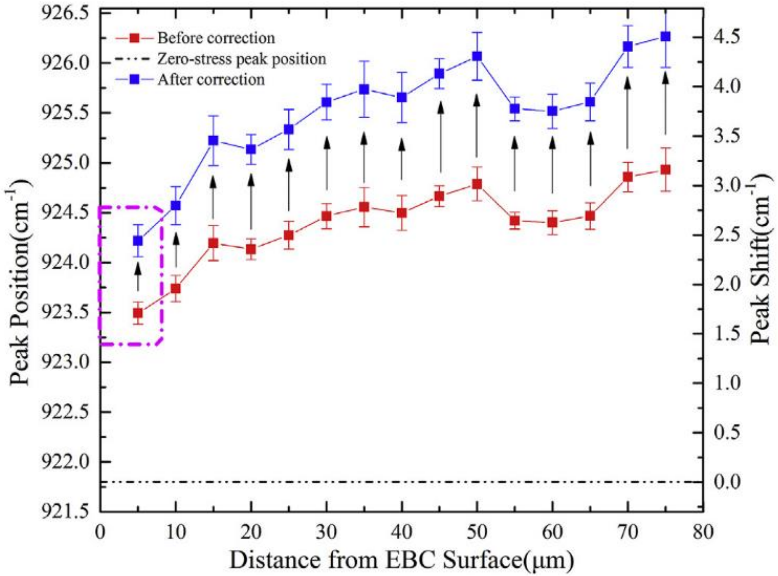

$Sin^2\Psi$ Stress Measurement

- Bruker D8 X-Ray diffractometer
  - Cu target
- Use plane as strain gauge
- $[\bar{2}20]$ plane selected
  - Strong intensity
  - Intermediate 2θ have higher accuracy
- Detector scanned $40° \leq 2\theta \leq 55°$
  - $[\bar{2}20]\ 2\theta = 47.000°$
- Slope of plot related to stress

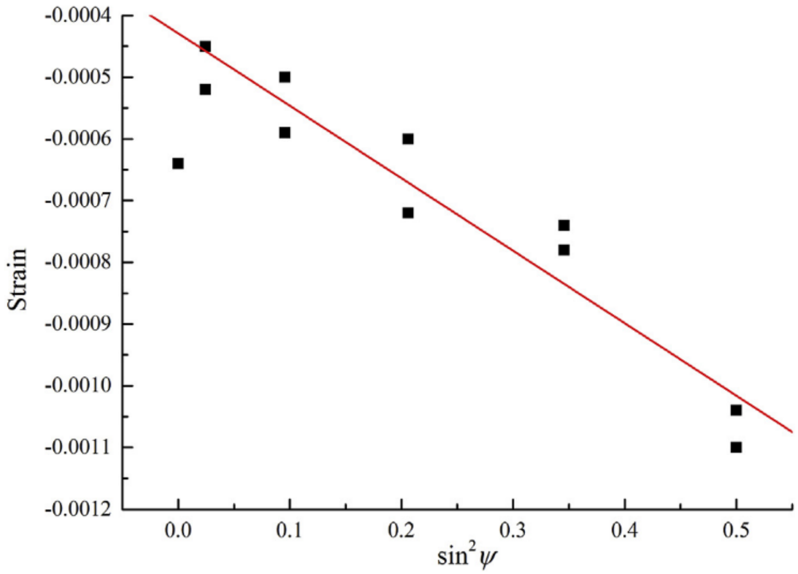

Residual Stress Determination

- Piezo spectroscopic relationship:

$$\Delta\nu_n = \frac{\Pi_n(\sigma_1 + \sigma_2 + \sigma_3)}{3}$$

  - $\Delta\nu_n$ - Peak shift
  - Π_n = Piezo-spectroscopic coefficient
  - σ = stresses in coating

- Edge effect – Poisson effect:

$$\sigma_B = \frac{\sigma_{edge}}{1 - \nu}$$

  - σ_B = Biaxial stress
  - σ_{edge}= Stress on free surface
  - ν = Poisson's ratio

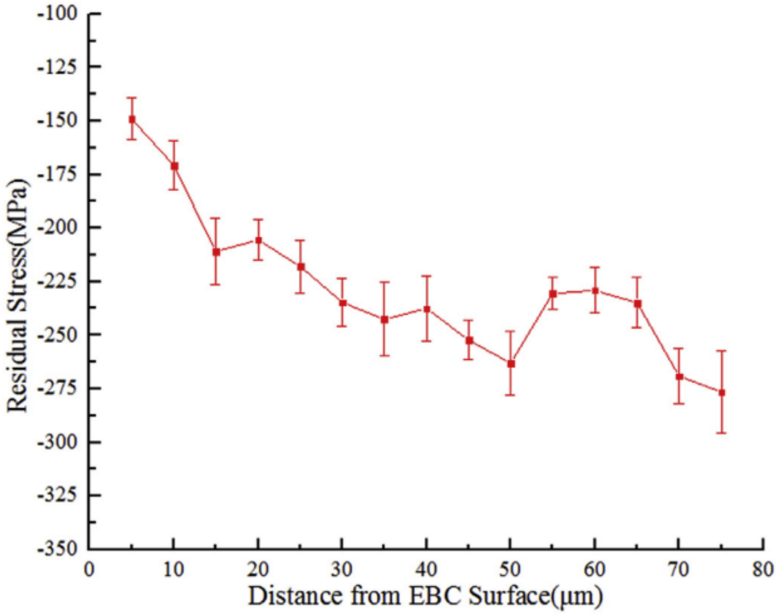

Reference(s): 22

Outline

- Introduction
- Background & Underlying Mechanisms
  - Ceramic Matrix Composites
  - Protective Coatings
  - Residual Stress in Coatings
  - X-Ray Diffraction – The $Sin^2\Psi$ Method
  - Raman Piezospectroscopy
- Summary of Work
- Critical Review
  - Insufficient Background
  - Reproducibility
  - Accuracy
  - Novelty & Impact
  - Suggested Improvements
- Conclusions

Impetus for Rare Earth EBCs

- APS & EB-PVD lead to lamellar & columnar microstructures of YSZ
  - Most common deposition techniques
  - Provide pathways for Ca-Mg-Al-Si (CMAS)

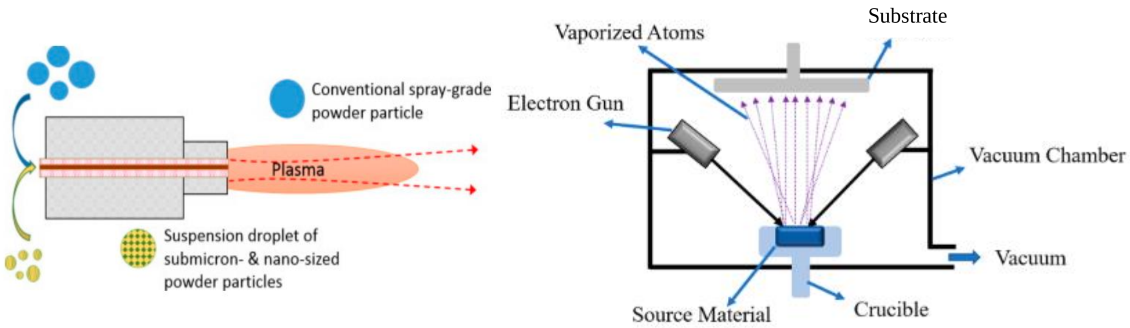

Figure from [30]

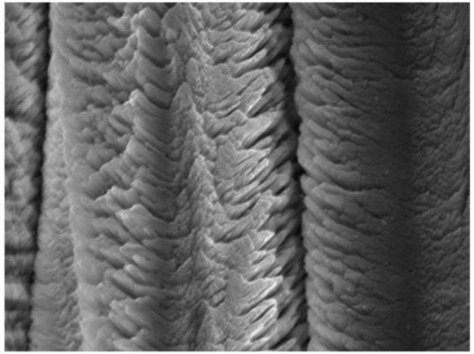

Columnar structure from [32]

Impetus for Rare Earth EBCs

- APS & EB-PVD lead to lamellar & columnar microstructures of YSZ
  - Most common deposition techniques
  - Provide pathways for Ca-Mg-Al-Si (CMAS)
- CMAS attack:
  - Sand, dust, ash, etc.
  - Melt ~1200 °C & penetrate pores / cracks
  - Causes stress upon solidification
  - Destabilizes YSZ
    - Zirconia allowed to undergo high temperature phase transformation

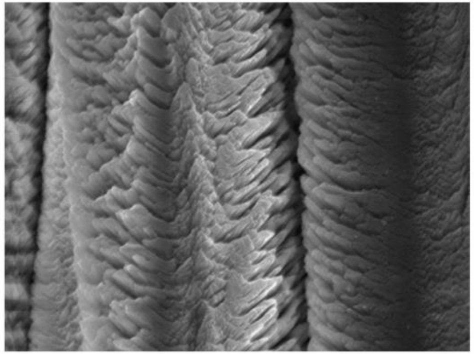

Columnar structure from [32]

Reference(s): 12,8,17,18,30,35,56

Impetus for Rare Earth EBCs

- Typical TBCs:
  - CMAS attack
  - Above 1100°C YSZ t'-tetragonal phase of YSZ will change to monoclinic and cubic phases which give rise to volumetric changes
- Si-based CMCs face volatilization:
  - ~1200 °C with $H_2O(g)$
  - ~1500 °C in O_2 for SiC & Si_3N_4

$$SiC + 1.5O_2(g) \rightarrow SiO_2 + CO(g)$$

$$SiO_2 + 2H_2O(g) \rightarrow Si(OH)_4(g)$$

Reference(s): 11,13,18,19

Impetus for Rare Earth EBCs

- Rare Earth Elements: Sc, Y, & the lanthanides
- YbDS is 3rd generation of EBC
  - RE / Mullite / Si / CMC
- CTE match with mullite & SiC:
  - β-$RE_2Si_2O_7$ & γ-$Y_2Si_2O_7$
  - ~4.0×10^{-6} K^{-1}
- $Lu_2Si_2O_7$ has SiO_2 on grain boundaries
- YbDS is leading candidate
  - Close CTE match
  - Single polymorph
  - Better CTE match & volatilization than Y_2SiO_5

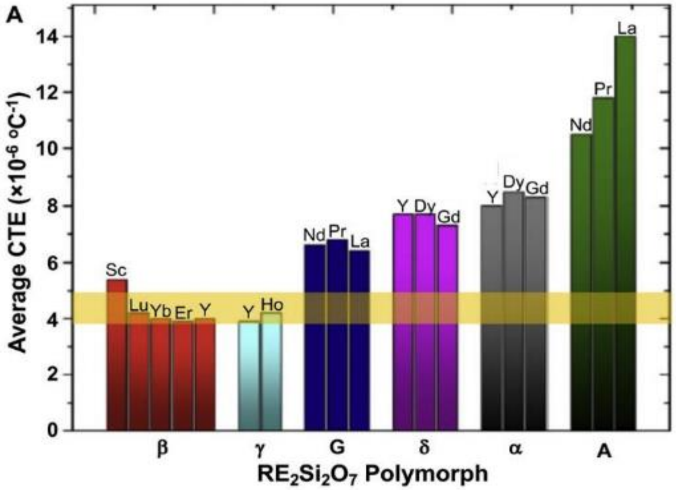

Figure from [13]

Residual Stresses in Coatings

- No description of the origin of residual stresses
- Thermal cycle stress, intrinsic stress, aging stress:

$$\sigma = \sigma_t + \sigma_{in} + \sigma_a$$

  - σ_t- CTE (α) mismatch leads to different volumes upon heating and cooling (ΔT)

$$\sigma_t = \frac{E_c}{1-\nu_c}(\alpha_c - \alpha_s)\Delta T$$

  - σ_{in} - ‘Growth stress’ from thermal mismatch, lattice mismatch, defects
  - σ_a- Changes in physical, mechanical, chemical properties over time
    - Sintering, oxidation, phase transformations
- Cracks, buckling → spallation, delamination, substrate exposure
  - Particularly concerning for TGO

Reference(s): 31,41,46,57

Reproducibility

- Scientific writing should be verifiable & reproducible
- Never reported Young's Modulus (*E*) or Poisson's ratio (ν)
  - $Sin^2\Psi$ method to determine surface stress
  - Edge stress correction (Biaxial modulus): $\sigma_B = \frac{\sigma_e}{1-\nu}$
- Missing standard deviation
  - $Sin^2\Psi$ plot fitting & measurements
  - Raman spectra fitting
- Surface stress from $Sin^2\Psi$ and PS coefficient are never reported

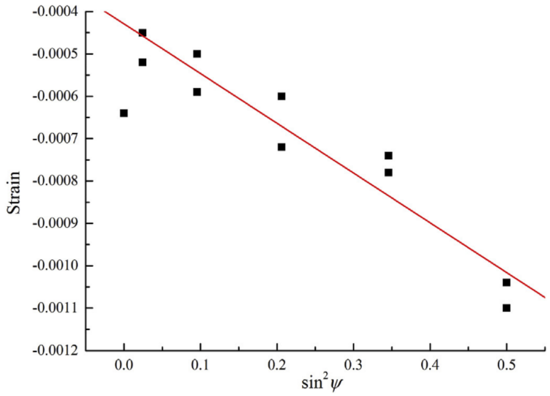

Reference(s): 22

Reproducibility

- Determine penetration depth of X-rays by linear attenuation coefficient

$$\mu \approx k\rho Z^3\lambda^3$$

  - ρ is density, Z is atomic number, λ is X-ray wavelength
  - No explanation of k or this relationship
  - No report of X-ray wavelength
  - ρ & Z are not straightforward
- Deposition conditions of slurry coating are missing
  - Residuals stresses are process dependent
  - Similar EBCs cannot be deposited to reproduce work

Reference(s): 31,41,46

Accuracy

- Claim compressive stress throughout coating

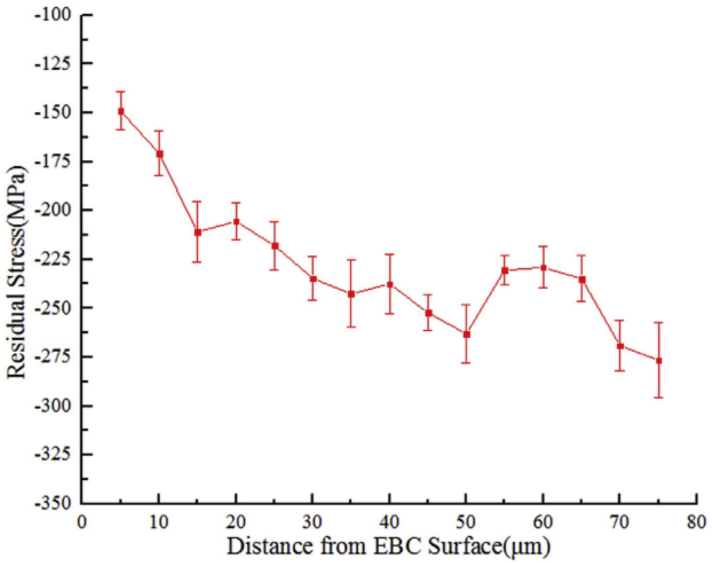

Reference(s): 22

Accuracy

- Claim compressive stress throughout coating
- "All peak shifts were positive in the top coat, indicating [compressive stress]"
  - Positive peak shift is not always compressive (Bouvier et al.)

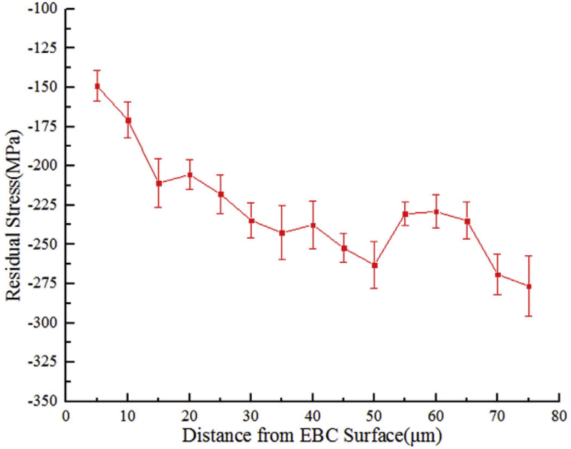

Figure from [52]

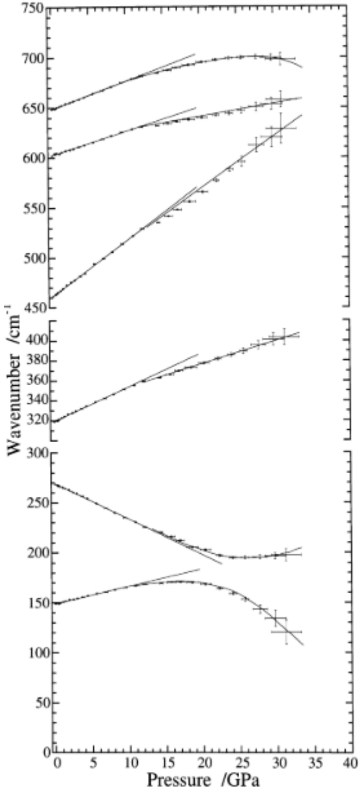

Reference(s): 22, 52

Accuracy

- Claim compressive stress throughout coating
- "All peak shifts were positive in the top coat, indicating [compressive stress]"
  - Positive peak shift is not always compressive (Bouvier et al.)
- Micropores within coating suggest tension
  - Conversely, micropores in TGO support compression

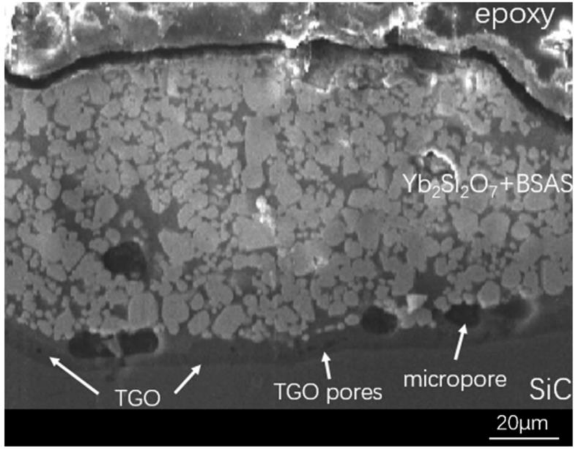

Accuracy

- Claim compressive stress throughout coating
- "All peak shifts were positive in the top coat, indicating [compressive stress]"
    - Positive peak shift is not always compressive (Bouvier et al.)
- Micropores within coating suggest tension
    - Conversely, micropores in TGO support compression
- No validation for values throughout coating
    - XRD near the top
    - Claim to match Richards et. al.
        - Finite element analysis which could have error

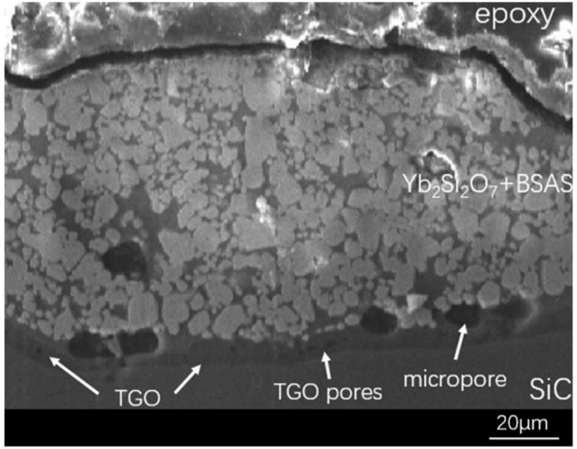

Accuracy

- $Sin^2\Psi$ method uses $2\theta \geq 125°$ to reduce error
  - Their $2\theta = 47.000°$
  - Reduce volume sampled of XRD sample
  - Glancing Incident XRD (GIXRD) used for thin films with low incident Ω
- "Good performance" from lack of cracks after testing
  - Significant difference from other experiments for similar coatings
  - Flowing 90% H_2O vapor and 10% O_2 with several cycles of high temperature
  - Silica / silica forming tubes & alumina tubes:
    - High internal $P_{Si(OH)4}$ & $P_{Al(OH)3}$
    - Artificially slow down corrosion rates
  - Not realistic testing environment

Reference(s): 18,31,35,36,40

Accuracy

- 1st & 2nd paragraph of *Experimental results and discussion*
- Claim their Equation 1 is valid for cubic crystals only

$$\Delta\nu_n = \frac{\Pi_n(\sigma_1 + \sigma_2 + \sigma_3)}{3}$$

  - Krämer et al. use it for polycrystalline zirconia
- Better represented as:

$$\Delta\nu_n = \frac{\Pi_n\langle\sigma_1 + \sigma_2 + \sigma_3\rangle}{3}$$

  - Stress term is averaged, PS coefficient represents uniaxial stress
- Raman piezo-spectroscopic (PS) coefficients
  - Dependent on applied stress when calibrated
  - Hydrostatic, biaxial, uniaxial:

$$\Pi_h = \frac{3}{2}\Pi_b = 3\Pi_u$$

Reference(s): 50-52,54,55,59

Accuracy

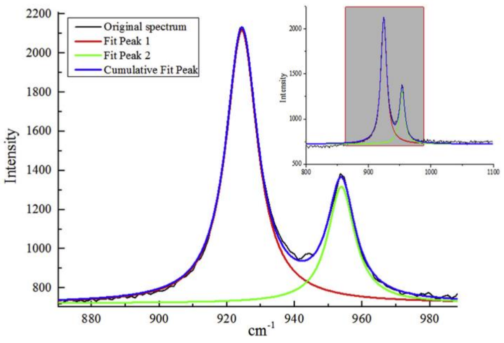

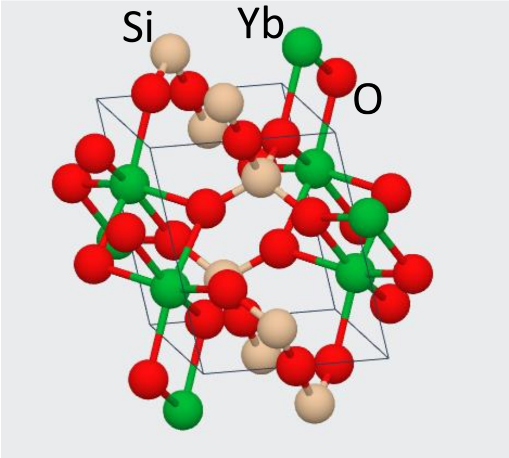

Figure from [62]

- Ye and Jiang indicate YbDS is monoclinic
  - Later claim, "… cubic structure of YbDS facilitated the calculation of residual stress through Equation (1)."
  - False & a contradiction
- Claim 921 cm^{-1} peak corresponds to Si-O-Si bending
  - Their own reference 22, Zheng et al. states in abstract that 500-700 cm^{-1} peaks are attributed to bending vibrations in $(SiO_4)^-$ tetrahedron
  - 800-1000 cm^{-1} range correspond to symmetric and antisymmetric stretching

Novelty & Impact

- Potential for improved efficiency & in-situ measurements
- Claim method of measuring stress is novel
  - Possibly first time determining PS coefficients through Raman & XRD explicitly
- Constable et al. correlated GIXRD $Sin^2\Psi$ stress to Raman peak shift
  - TlAl/VN coatings on stainless steel substrates
- Tomaszewski et al. proposed indirect method of determining PS coefficients
  - Suggested using different techniques to determine stress
  - f is volume fraction

$$f_1\langle\sigma\rangle_1 + f_2\langle\sigma\rangle_2 = 0 \Rightarrow \Pi_2 = -\frac{f_2\Delta\nu_2}{f_1\langle\sigma\rangle_1}$$

Reference(s): 41,54

Novelty & Impact

- Ye & Jiang's method is destructive
- Loechelt et al. - determine stress tensor without calibration
  - Polarize laser & tilt detector off axis
  - Sample different Raman active phonons to deconvolute phonon splitting and mixing

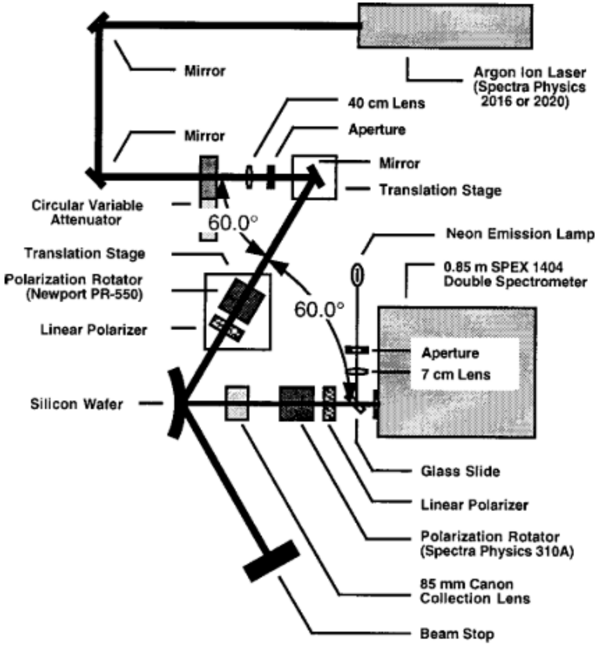

Figure from [64]

Novelty & Impact

- Ye & Jiang's method is destructive
- Loechelt et al. - determine stress tensor without calibration
  - Polarize laser & tilt detector off axis
  - Sample different Raman active phonons to deconvolute phonon splitting and mixing
- Ohtsuka et al. used confocal microscope to measure depth-dependent stress
  - Al_2O_3 coating on Si_3N_4 substrate

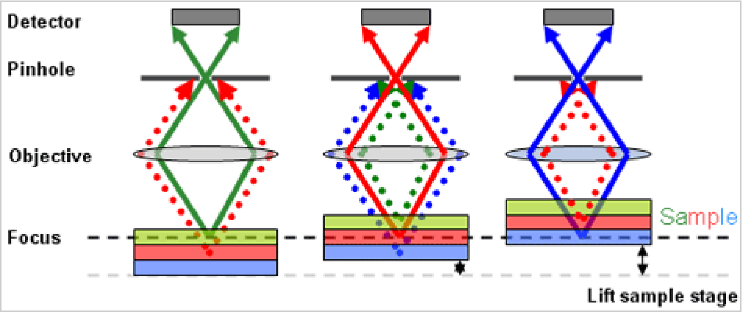

Figure from M.S. thesis presentation

Suggested Improvements

- Report values used in calculations
- Report details on coating deposition
  - Residual stresses vary depending on deposition
- Validate measurements
  - Determine PS coefficients through calibration
  - Use well-studied materials with established PS coefficients
- Demonstrate before & after SEM images
  - Aid in evaluation of performance under these testing conditions
  - Microstructure evolution

Suggested Improvements

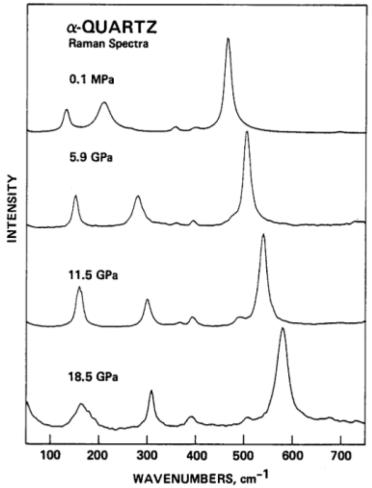

- Raman spectroscopy:
  - Show entire Raman spectra – powder & sample
  - Pick a peak which is not convoluted with another peak
- Reorganize paper structure
  - Figures referenced after they appear
  - Large amount of white space
- Be consistent on Lorentz vs. Lorenz fitting
- Demonstrate diagrams for XRD and stresses

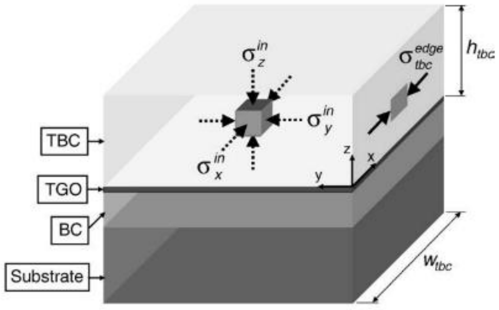

Reference(s): 32,65

Figures from [32] and [65]

Suggested Improvements

- Use $Sin^2\Psi$ along depth as calibration method
  - Depends on spatial resolution of XRD
- BSAS has high temperature phase transition
  - ~1590 °C
  - Present due to deposition parameters
  - Persistent below transition temperature for extended periods
- Determining unstressed Raman spectra with different deposition
  - Chemical reaction between materials
  - Indistinct grains or bonds

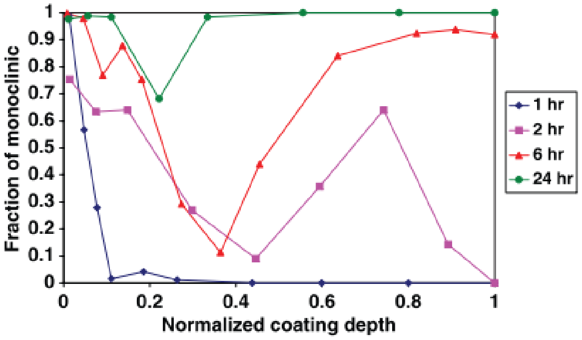

BSAS phase from [31] @1400 °C

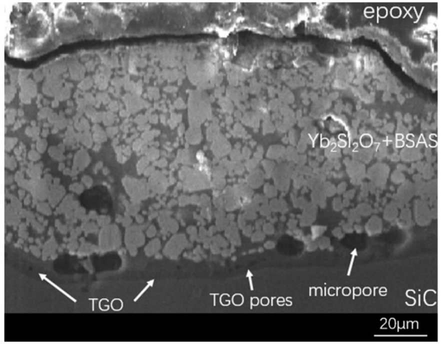

Reference(s): 31

Conclusions

- CMCs combined with EBCs are promising
  - Residual stresses are a significant challenge
  - Requires reliable measurement techniques
- Ye & Jiang’s work represents efficient & promising method
  - No calibration required
  - In-situ measurements
- Work suffers from lack of reproducibility
- Requires validation

Reference(s):

Questions?

- Thank you for serving on my committee

References

[1] S. Bose, “Introduction,” in *High Temperature Coatings*, vol. 12, no. 1, Elsevier, 2018, pp. 1–6.

[2] L. K. Mansur, A. F. Rowcliffe, R. K. Nanstad, S. J. Zinkle, W. R. Corwin, and R. E. Stoller, “Materials needs for fusion, Generation IV fission reactors and spallation neutron sources - Similarities and differences,” *J. Nucl. Mater.*, vol. 329–333, no. 1-3 PART A, pp. 166–172, 2004.

[3] S. X. Mao, “Impermeable thin Al 2 O 3 overlay for TBC protection from sulfate and vanadate attack in gas turbines,” Pittsburgh, PA, 2003.

[4] “Materials for Harsh Service Conditions Chapter 6: Technology Assesments,” 2015.

[5] F. Garciá Ferré *et al.*, “Radiation endurance in Al2O3 nanoceramics,” *Sci. Rep.*, vol. 6, no. September, pp. 1–10, 2016.

[6] Y. Ueki, T. Kunugi, M. Kondo, A. Sagara, N. B. Morely, and M. A. Abdou, “Consideration of Alumina Coating Fabricated by Sol-gel Method as MHD Coating against PbLi,” in *Proceedings of the 13th International Topical Meeting on Nuclear Reactor Thermal Hydraulics*, 2009, pp. 1–10.

[7] M. Nuri Rahuma and B. Kannan M, “Corrosion in Oil and Gas Industry: A Perspective on Corrosion Inhibitors,” *J. Mater. Sci. Eng.*, vol. 03, no. 03, p. 4172, 2014.

[8] M. Belmonte, “Advanced ceramic materials for high temperature applications,” *Adv. Eng. Mater.*, vol. 8, no. 8, pp. 693–703, 2006.

[9] A. Hasegawa, A. Kohyama, R. H. Jones, L. L. Snead, B. Riccardi, and P. Fenici, “Critical issues and current status of SiC/SiC composites for fusion,” *J. Nucl. Mater.*, vol. 283, no. 287, pp. 128–137, 2000.

[10] V. Rubio *et al.*, “Thermal properties and performance of carbon fiber-based ultra-high temperature ceramic matrix composites (Cf-UHTCMCs),” *J. Am. Ceram. Soc.*, vol. 103, no. 6, pp. 3788–3796, 2020.

[11] R. Raj, “Fundamental Research in Structural Ceramics for Service Near 2000°C,” *J. Am. Ceram. Soc.*, vol. 76, no. 9, pp. 2147–2174, 1993.

[12] Y. Xu, X. Hu, F. Xu, and K. Li, “Rare earth silicate environmental barrier coatings: Present status and prospective,” *Ceram. Int.*, vol. 43, no. 8, pp. 5847–5855, 2017.

[13] T. H. Daniel Tejero-Martin, Chris Bennett, “A Review on Environmental Barrier Coatings: History, Current State of the Art and Future Developments,” 2020.

[14] H. Ohnabe, S. Masaki, M. Onozuka, K. Miyahara, and T. Sasa, “Potential application of ceramic matrix composites to aero-engine components,” *Compos. Part A Appl. Sci. Manuf.*, vol. 30, no. 4, pp. 489–496, 1999.

[15] K. K. Chawla, “Ceramic Matrix Composites,” in *Composite Materials*, vol. 43, no. 4, Cham: Springer International Publishing, 2019, pp. 251–296.

[16] S. Bose, “Thermal Barrier Coatings (TBCs),” in *High Temperature Coatings*, Elsevier, 2018, pp. 199–299.

[17] D. R. Clarke and C. G. Levi, “Materials Design for the Next Generation Thermal Barrier Coatings,” *Annu. Rev. Mater. Res.*, vol. 33, no. 1, pp. 383–417, Aug. 2003.

[18] B. T. Richards, S. Sehr, F. De Franqueville, M. R. Begley, and H. N. G. Wadley, “Fracture mechanisms of ytterbium monosilicate environmental barrier coatings during cyclic thermal exposure,” *Acta Mater.*, vol. 103, pp. 448–460, 2016.

[19] K. N. Lee, “Current status of environmental barrier coatings for Si-based ceramics,” *Surf. Coatings Technol.*, vol. 133–134, pp. 1–7, 2000.

[20] V. Teixeira, M. Andritschky, W. Fischer, H. P. Buchkremer, and D. Stöver, “Analysis of residual stresses in thermal barrier coatings,” *J. Mater. Process. Technol.*, vol. 92–93, pp. 209–216, 1999.

[21] Y. H. Sohn, B. Jayaraj, S. Laxman, B. Franke, J. W. Byeon, and A. M. Karlsson, “The non-destructive and nano-microstructural characterization of thermal-barrier coatings,” *JOM*, vol. 56, no. 10, pp. 53–56, Oct. 2004.

[22] C. Ye and P. Jiang, “Accurate residual stress measurement as a function of depth in environmental barrier coatings via a combination of X-ray diffraction and Raman spectroscopy,” *Ceram. Int.*, vol. 46, no. 8, pp. 12613–12617, 2020.

References

[23] A. Sommers, Q. Wang, X. Han, C. T'Joen, Y. Park, and A. Jacobi, "Ceramics and ceramic matrix composites for heat exchangers in advanced thermal systems-A review," *Appl. Therm. Eng.*, vol. 30, no. 11–12, pp. 1277–1291, 2010.

[24] J. Cho, A. R. Boccaccini, and M. S. P. Shaffer, "Ceramic matrix composites containing carbon nanotubes," *J. Mater. Sci.*, vol. 44, no. 8, pp. 1934–1951, 2009.

[25] D. Han, H. Mei, S. Xiao, K. G. Dassios, and L. Cheng, "A review on the processing technologies of carbon nanotube/silicon carbide composites," *J. Eur. Ceram. Soc.*, vol. 38, no. 11, pp. 3695–3708, 2018.

[26] T. F. Cooke, "Inorganic Fibers-A Literature Review," *J. Am. Ceram. Soc.*, vol. 74, no. 12, pp. 2959–2978, Dec. 1991.

[27] S. Schmidt, S. Beyer, H. Knabe, H. Immich, R. Meistring, and A. Gessler, "Advanced ceramic matrix composite materials for current and future propulsion technology applications," *Acta Astronaut.*, vol. 55, no. 3–9, pp. 409–420, 2004.

[28] M. Klaus, C. Genzel, and H. Holzschuh, "Residual stress depth profiling in complex hard coating systems by X-ray diffraction," *Thin Solid Films*, vol. 517, no. 3, pp. 1172–1176, 2008.

[29] E. Alat, A. T. Motta, R. J. Comstock, J. M. Partezana, and D. E. Wolfe, "Ceramic coating for corrosion (c3) resistance of nuclear fuel cladding," *Surf. Coatings Technol.*, vol. 281, pp. 133–143, 2015.

[30] B. Fotovvati, N. Namdari, and A. Dehghanghadikolaei, "On Coating Techniques for Surface Protection: A Review," *J. Manuf. Mater. Process.*, vol. 3, no. 1, p. 28, 2019.

[31] K. N. Lee, J. I. Eldridge, and R. C. Robinson, "Residual stresses and their effects on the durability of environmental barrier coatings for SiC ceramics," *J. Am. Ceram. Soc.*, vol. 88, no. 12, pp. 3483–3488, 2005.

[32] M. Tanaka, R. Kitazawa, T. Tomimatsu, Y. F. Liu, and Y. Kagawa, "Residual stress measurement of an EB-PVD Y2O3-ZrO2 thermal barrier coating by micro-Raman spectroscopy," *Surf. Coatings Technol.*, vol. 204, no. 5, pp. 657–660, 2009.

[33] S. Ramasamy, S. N. Tewari, K. N. Lee, R. T. Bhatt, and D. S. Fox, "Environmental durability of slurry based mullite-gadolinium silicate EBCs on silicon carbide," *J. Eur. Ceram. Soc.*, vol. 31, no. 6, pp. 1123–1130, 2011.

[34] S. Ramasamy, S. N. Tewari, K. N. Lee, R. T. Bhatt, and D. S. Fox, "EBC development for hot-pressed Y2O3/Al2O3 doped silicon nitride ceramics," *Mater. Sci. Eng. A*, vol. 527, no. 21–22, pp. 5492–5498, 2010.

[35] S. Ramasamy, S. N. Tewari, K. N. Lee, R. T. Bhatt, and D. S. Fox, "Slurry based multilayer environmental barrier coatings for silicon carbide and silicon nitride ceramics - I. Processing," *Surf. Coatings Technol.*, vol. 205, no. 2, pp. 258–265, 2010.

[36] S. Ramasamy, S. N. Tewari, K. N. Lee, R. T. Bhatt, and D. S. Fox, "Slurry based multilayer environmental barrier coatings for silicon carbide and silicon nitride ceramics — II. Oxidation resistance," *Surf. Coatings Technol.*, vol. 205, no. 2, pp. 266–270, Oct. 2010.

[37] J. I. Federer, "Alumina base coatings for protection of SiC ceramics," *J. Mater. Eng.*, vol. 12, no. 2, pp. 141–149, Jun. 1990.

[38] T. Suetsuna, M. Ishizaki, M. Ando, N. Kondo, T. Ohji, and S. Kanzaki, "Lutetium disilicate coating on silicon nitride for high temperature oxidation resistance," *J. Ceram. Soc. Japan*, vol. 112, no. 1305, pp. 301–304, 2004.

[39] D. D. Jayaseelan, S. Ueno, T. Ohji, and S. Kanzaki, "Sol-gel synthesis and coating of nanocrystalline Lu2Si 2O7 on Si3N4 substrate," *Mater. Chem. Phys.*, vol. 84, no. 1, pp. 192–195, 2004.

[40] Q. Luo and S. Yang, "Uncertainty of the X-ray Diffraction (XRD) sin2 ψ Technique in Measuring Residual Stresses of Physical Vapor Deposition (PVD) Hard Coatings," *Coatings*, vol. 7, no. 8, p. 128, Aug. 2017.

References

[41] C. P. Constable, D. B. Lewis, J. Yarwood, and W. D. Münz, "Raman microscopic studies of residual and applied stress in PVD hard ceramic coatings and correlation with X-ray diffraction (XRD) measurements," *Surf. Coatings Technol.*, vol. 184, no. 2–3, pp. 291–297, 2004.

[42] P. Jiang, X. Fan, Y. Sun, H. Wang, L. Su, and T. Wang, "Thermal-cycle dependent residual stress within the crack-susceptible zone in thermal barrier coating system," *J. Am. Ceram. Soc.*, vol. 101, no. 9, pp. 4256–4261, 2018.

[43] B. J. Harder, J. D. Almer, C. M. Weyant, K. N. Lee, and K. T. Faber, "Residual stress analysis of multilayer environmental barrier coatings," *J. Am. Ceram. Soc.*, vol. 92, no. 2, pp. 452–459, 2009.

[44] O. ANDEROGLU, "RESIDUAL STRESS MEASUREMENT USING X-RAY DIFFRACTION," Texas A & M, 2004.

[45] S. Bose, "Nondestructive Inspection (NDI) of Coatings," in *High Temperature Coatings*, Elsevier, 2018, pp. 301–318.

[46] I. A. Alhomoudi and G. Newaz, "Residual stresses and Raman shift relation in anatase TiO2 thin film," *Thin Solid Films*, vol. 517, no. 15, pp. 4372–4378, 2009.

[47] T. Tomimatsu, S. J. Zhu, and Y. Kagawa, "Local stress distribution in thermally-grown-oxide layer by near-field optical microscopy," *Scr. Mater.*, vol. 50, no. 1, pp. 137–141, 2004.

[48] I. C. Noyan, T. C. Huang, and B. R. York, "Residual stress/strain analysis in thin films by X-ray diffraction," *Crit. Rev. Solid State Mater. Sci.*, vol. 20, no. 2, pp. 125–177, Jan. 1995.

[49] Q. Chen, W. G. Mao, Y. C. Zhou, and C. Lu, "Effect of Young's modulus evolution on residual stress measurement of thermal barrier coatings by X-ray diffraction," *Appl. Surf. Sci.*, vol. 256, no. 23, pp. 7311–7315, 2010.

[50] S. Ohtsuka, W. Zhu, S. Tochino, Y. Sekiguchi, and G. Pezzotti, "In-depth analysis of residual stress in an alumina coating on silicon nitride substrate using confocal Raman piezo-spectroscopy," *Acta Mater.*, vol. 55, no. 4, pp. 1129–1135, 2007.

[51] A. M. Limarga and D. R. Clarke, "Piezo-spectroscopic coefficients of tetragonal-prime yttria-stabilized zirconia," *J. Am. Ceram. Soc.*, vol. 90, no. 4, pp. 1272–1275, 2007.

[52] P. Bouvier and G. Lucazeau, "Raman spectra and vibrational analysis of nanometric tetragonal zirconia under high pressure," *J. Phys. Chem. Solids*, vol. 61, no. 4, pp. 569–578, 2000.

[53] W. G. Mao, Q. Chen, C. Y. Dai, L. Yang, Y. C. Zhou, and C. Lu, "Effects of piezo-spectroscopic coefficients of 8wt.% Y2O3 stabilized ZrO2 on residual stress measurement of thermal barrier coatings by Raman spectroscopy," *Surf. Coatings Technol.*, vol. 204, no. 21–22, pp. 3573–3577, 2010.

[54] H. Tomaszewski, J. Strzeszewski, L. Adamowicz, and V. Sergo, "Indirect Determination of the Piezospectroscopic Coefficients of Ceria-Stabilized Tetragonal Zirconia Polycrystals," *J. Am. Ceram. Soc.*, vol. 85, no. 11, pp. 2855–2857, 2002.

[55] M. Tanaka, M. Hasegawa, A. F. Dericioglu, and Y. Kagawa, "Measurement of residual stress in air plasma-sprayed Y2 O3-ZrO2 thermal barrier coating system using micro-Raman spectroscopy," *Mater. Sci. Eng. A*, vol. 419, no. 1–2, pp. 262–268, 2006.

[56] G. Pujol, F. Ansart, J.-P. Bonino, A. Malié, and S. Hamadi, "Step-by-step investigation of degradation mechanisms induced by CMAS attack on YSZ materials for TBC applications," *Surf. Coatings Technol.*, vol. 237, pp. 71–78, Dec. 2013.

[57] J. Narayan, "Recent progress in thin film epitaxy across the misfit scale (2011 Acta Gold Medal Paper)," *Acta Mater.*, vol. 61, no. 8, pp. 2703–2724, 2013.

[58] S. Bose, "Fundamental Concepts," in *High Temperature Coatings*, Elsevier, 2018, pp. 7–27.

References

[59] S. Krämer *et al.*, “Mechanisms of cracking and delamination within thick thermal barrier systems in aero-engines subject to calcium-magnesium-alumino-silicate (CMAS) penetration,” *Mater. Sci. Eng. A*, vol. 490, no. 1–2, pp. 26–35, 2008.

[60] J. R. Ferraro, K. Nakamoto, and C. W. Brown, “Basic Theory,” in *Introductory Raman Spectroscopy*, Elsevier, 2003, pp. 1–94.

[61] B. A. Kanies, “An investigation into the effects of ion tracks on α -quartz,” Missouri University of Science and Technology, 2018.

[62] K. Persson, “Materials Data on Yb2Si2O7 (SG:12) by Materialsle,” 2016. [Online]. Available: https://materialsproject.org/materials/mp-4300/. [Accessed: 30-Aug-2020].

[63] L. Zheng *et al.*, “Raman spectroscopic investigation of pure and ytterbium-doped rare earth silicate crystals,” *J. Raman Spectrosc.*, vol. 38, no. 11, pp. 1421–1428, Nov. 2007.

[64] G. H. Loechelt, N. G. Cave, and J. Menéndez, “Polarized off-axis Raman spectroscopy: A technique for measuring stress tensors in semiconductors,” *J. Appl. Phys.*, vol. 86, no. 11, pp. 6164–6180, 1999.

[65] R. J. Hemley, “Pressure Dependence of Raman Spectra SiO2 Plymorphs: alpha-Quartz, Coesite, and Stishovofite,” in *High-Pressure Research in Mineral Physics*, M. Manghnani and Y. Syono, Eds. Tokyo, Japan: Terra Scientific Publishing Company, 1987, pp. 347–359.

Reference(s):